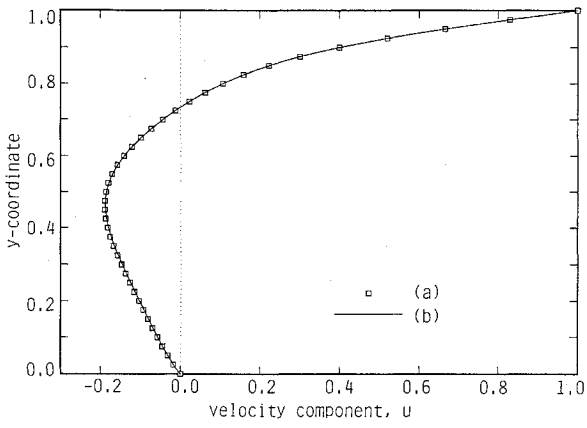

Fig. 1 Horizontal velocity component along the vertical centerline at Re = 400: a) present scheme and b) Beam and Warming scheme.

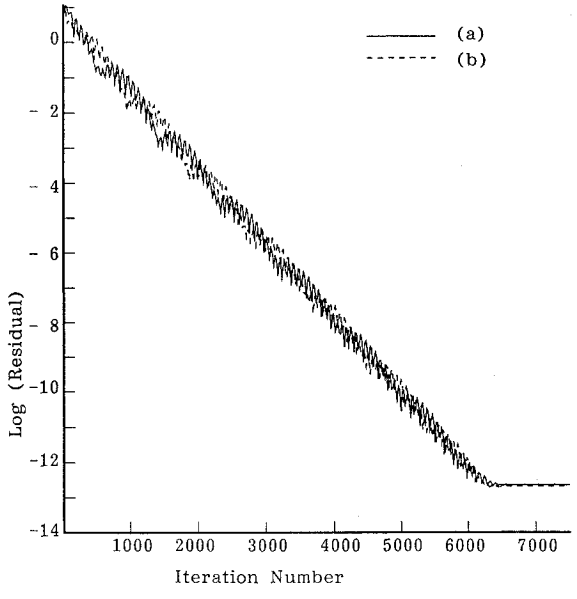

Fig. 2 Convergence history at Re = 400: a) present scheme and b) Beam and Warming scheme.

Comparisons of the computed results with numerical results obtained by the Beam and Warming scheme[4] are shown in Fig. 1. The convergence histories for our scheme and the Beam and Warming scheme are also shown in Fig. 2. These comparisons of the computed velocity and the convergence histories confirm the analytical developments of our scheme.

Conclusions

An implicit scheme is developed for the solution of the Navier–Stokes equations (compressible and incompressible). This scheme is based upon the superposition of several one-dimensional solutions which are independent of one another. Therefore, these one-dimensional solutions can be computed simultaneously on separate processors (parallel processing). Also, separate processors may be employed for each coordinate direction. The maximum number of processors which can be employed in each coordinate direction is limited by the maximum number of grid points in each direction. For example, consider a two-dimensional problem with $(M \times N)$ grid lines, the maximum number of processors that can be employed is $k(M + N - 4)$ processors where k is the number of equations. In addition, the present scheme has the advantage that no boundary conditions are needed for the one-dimensional solutions. This is because the boundary conditions on the physical velocity field are implemented in the governing equations before the superposition step takes place. The computed results for the driven cavity problem confirm the analytical developments of the present scheme.

Acknowledgment

This work was sponsored by the Office of Naval Research.

References

[1]Anderson, D. A., Tannehill, J. C., and Pletcher, R. H., *Computational Fluid Mechanics and Heat Transfer*, McGraw-Hill, 1984, pp. 88–97.
[2]Roache, P. J., *Computational Fluid Dynamics*, Hermosa, Albuquerque, NM, 1976, pp. 36–75.
[3]Jameson, A., "Numerical Solution of the Euler Equations by Finite Volume Methods Using Runge-Kutta Time-Stepping Schemes," AIAA Paper 81-1259, June 1981.
[4]Beam, R., and Warming, R. F., "An Implicit Factored Scheme for the Compressible Navier–Stokes Equations," *AIAA Journal*, Vol. 16, No. 4, 1978, p. 393.
[5]Sotiropoulos, F., and Abdallah, S., "A Primitive Variable Method for the Solution of Three-Dimensional Incompressible Viscous Flows," *Journal of Computational Physics*, Vol. 103, No. 2, 1992, pp. 336–349.
[6]Larson, L., Patel, V. C., and Gilbert, D. (eds.), *Ship Viscous Flow*, Proceedings of 1990 SSPA Maritime Consulting AB—Chalmers University of Technology—Iowa Institute of Hydraulic Research Workshop, Flowtech International AB, Gothenburg, Sweden, 1990, pp. 8–16.
[7]Steger, J. L., "Implicit Finite Difference Simulation of Flow About Arbitrary Two-Dimensional Geometries," *AIAA Journal*, Vol. 16, No. 7, 1978, pp. 679–686.
[8]Abdallah, S., "Numerical Solutions for the Pressure Poisson Equation with Neumann Boundary Conditions Using a Non-Staggered Grid, I" *Journal of Computational Physics*, Vol. 70, No. 1, 1987, pp. 182–192.
[9]Abdallah, S., "Numerical Solutions for the Incompressible Navier–Stokes Equations in Primitive Variables Using a Non-Staggered Grid, II," *Journal of Computational Physics*, Vol. 70, No. 1, 1987, pp. 193–203.

Effects of Spatial Order of Accuracy on the Computation of Vortical Flowfields

J. A. Ekaterinaris*
Navy-NASA Joint Institute of Aeronautics, Moffett Field, California 94035

Introduction

ACCURATE prediction of subsonic, vortical flows over swept wings, slender bodies, and slender body/delta wing combinations at high incidence is of interest to aerodynamicists. The main characteristic of the flow over a swept wing at high incidence is the leading-edge vortex. This vortex is formed by the windward and leeward-side boundary layers which separate at the leading-edge and roll up in a helical fashion. For many practical applications, such as flows over a full aircraft or a canard-wing configuration, the leading-edge vortices generated by a slender wing convect downstream. It is, therefore, important for numerical methods to predict correctly the strength of these vortices and convect them downstream with minimal diffusion, because their presence significantly affects the development of the downstream flowfield.

Numerical methods currently used, such as second-order central difference and upwind schemes, require high grid resolution close to the surface to predict the viscous flow region accurately. In addition, adequate grid density is required in the vortical-flow region to resolve the complex flowfield features. Numerical simulations for flows over delta wings (cf. Refs. 1–4) showed that the lifting characteristics and surface pressure distributions are predicted accurately

Received June 20, 1993; presented as Paper 93-3371 at the AIAA 11th Computational Fluid Dynamics Conference, Orlando, FL, July 6–9, 1993; revision received June 5, 1994; accepted for publication June 6, 1994.

*Research Associate Professor, Naval Postgraduate School, Department of Aeronautics and Astronautics. Senior Member AIAA.

with a reasonable number of grid points. However, higher grid resolution is required to predict the vorticity and the velocity gradients in the vortex cores. Several investigators[3,5,6] used embedded grids to obtain better resolution of the vortical-flow region.

The vortical flowfield generated by the flow over a double-delta wing was previously investigated.[4] An important feature of this flowfield is the interaction between the strake vortex, after it convects over the wing, with the wing primary vortex. It was found that the overall quality of the predictions depends significantly on how well the strake vortex could be convected downstream of the strake section by the numerical solution. Solutions on refined grids[4] showed that small improvements can be obtained with grid refinement only in the circumferential direction. In Ref. 4 it was found that the strake vortex lifts away from the surface with increasing angle of incidence, vortex interaction becomes stronger, and, as a result, the predictions of the surface pressure distributions deteriorate. To convect the strake vortex properly the grid must be refined in all three directions in the vortical-flow region. It was observed, however, in Ref. 4 that increased order of accuracy for the evaluation of the inviscid fluxes improved the numerical solutions. In this study an attempt is made to evaluate more systematically how increased order of accuracy affects the numerical solution.

The objective of the present investigation is to assess the effect of the spatial order of accuracy used for the evaluation of the inviscid fluxes on the resolution of higher order quantities, such as velocity gradients. The viscous terms are computed as second-order accurate with central difference formulas, even though for the explicit part of the algorithm higher order approximations may be used. A viscous/inviscid zonal method is used, and the outer part of the flowfield is computed with the inviscid flow equations. The viscous boundary-layer type flow region close to the body surface is computed with an algebraic eddy viscosity model.[7] Results obtained with the conservative and nonconservative formulations and the viscous/inviscid approach are compared with available experimental data. The effect of grid refinement on the accuracy of the solution is also presented.

Governing Equations

The conservative form of the compressible, thin-layer Navier-Stokes equations is used to compute the near-wall flowfield. The full details of the conservative formulation and the solution method are given in Ref. 4. The primitive variable formulation of the inviscid governing equations is used for the computation of the outer part of the flowfield. The differential form of these equations for an arbitrary coordinate system (ξ, η, ζ) can be written as

$$\partial_t \boldsymbol{q} + A\partial_\xi \boldsymbol{q} + B\partial_\eta \boldsymbol{q} + C\partial_\zeta \boldsymbol{q} = 0 \tag{1}$$

where $\boldsymbol{q}$ is the vector of the primitive variables, $\boldsymbol{q} = (\rho, u, v, w, p)^T$; ρ is the density; u, v, and w are the Cartesian velocity components; and p is the pressure. The matrices A, B, and C are obtained from matrix D

$$D = \begin{pmatrix} U & \rho k_x & \rho k_y & \rho k_z & 0 \\ 0 & U & 0 & 0 & k_x/\rho \\ 0 & 0 & U & 0 & k_y/\rho \\ 0 & 0 & 0 & U & k_z/\rho \\ 0 & \rho a^2 k_x & \rho a^2 k_y & \rho a^2 k_z & U \end{pmatrix} \tag{2}$$

In Eq. (2) U is a contravariant component, and k_x, k_y, k_z are metric terms. For example, k_x, k_y, and k_z are ξ_x, ξ_y, and ξ_z for matrix A.

Numerical Scheme

The solution for the viscous inner zone is obtained with the conservative formulation of the governing equations. For this case, the numerical scheme is described in detail in Ref. 4. For the inviscid outer zone, explicit time integration can be obtained with a fourth-order Runge-Kutta scheme. This scheme yields better stability limits compared to an Euler explicit scheme. The fourth-order Runge-Kutta scheme is as follows: $\boldsymbol{q}^0 = \boldsymbol{q}^n$, $\boldsymbol{q}^1 = \boldsymbol{q}^0 - (\Delta t/2)R(q^0)$, $\boldsymbol{q}^2 = \boldsymbol{q}^0 - (\Delta t/2)R(q^1)$, $\boldsymbol{q}^3 = \boldsymbol{q}^0 - \Delta t R(q^2)$, $\boldsymbol{q}^4 = \boldsymbol{q}^0 - (\Delta t/6)\{R(q^0) + 2R(q^1) + 2R(q^2) + R(q^3)\}$, $\boldsymbol{q}^{n+1} = \boldsymbol{q}$ (Ref. 4).

The Courant, Isaacson, Rees (CIR) method,[8] generalized in Ref. 9 as the split-coefficient matrix (SCM) method, is used to evaluate the inviscid fluxes. Using the SCM method, the right-hand-side residual R is evaluated as

$$R = \left(A^+ q_\xi^- + A^- q_\xi^+\right) + \left(B^+ q_\eta^- + B^- q_\eta^+\right) + \left(C^+ q_\zeta^- + C^- q_\zeta^+\right) \tag{3}$$

The matrices $A^\pm = T\Lambda^\pm T^{-1}$ etc. are computed as in Ref. 9.

To enable time-accurate solutions with highly stretched grids, an implicit integration scheme may be used. Implicit time integration is obtained with the trapezoidal integration rule and an approximately factorized scheme as follows:

$$\begin{aligned} &[I + \Delta t(A^+\nabla_\xi + A^-\Delta_\xi)]^p \times [I + \Delta t(B^+\nabla_\eta + B^-\Delta_\eta)]^p \\ &\quad \times [I + \Delta t(C^+\nabla_\zeta + C^-\Delta_\zeta)]^p \times (\boldsymbol{q}^{p+1} - \boldsymbol{q}^p) \\ &\quad = -\Delta t \left\{ \frac{\boldsymbol{q}^p - \boldsymbol{q}^n}{\Delta t} + (A^+ q_\xi^- + A^- q_\xi^+) \right. \\ &\quad \left. + (B^+ q_\eta^- + B^- q_\eta^+) + (C^+ q_\zeta^- + C^- q_\zeta^+) \right\}^p \end{aligned} \tag{4}$$

To retain a block tridiagonal structure, the first-order backward ($\nabla y = y_i - y_{i-1}$) and forward ($\Delta y = y_{i+1} - y_i$) operators are used on the left-hand side of Eq. (4). The implicit part of the algorithm is linearized using the same method as the explicit part, and the Newton subiterations, indicated by the iteration index p in Eq. (4), may be set to zero. The right-hand-side explicit terms, q_ξ^+, q_ξ^-, are evaluated using higher order, upwind-biased finite difference operators. For third-order accuracy, the following formulas are used:

$$\begin{aligned} q_\xi^+ &= \tfrac{1}{6}(-q_{i+2} + 6q_{i+1} - 3q_i - 2q_{i-1}) \\ q_\xi^- &= \tfrac{1}{6}(+2q_{i+1} + 3q_i - 6q_{i-1} + q_{i-2}) \end{aligned} \tag{5}$$

For fourth-order accuracy,

$$\begin{aligned} q_\xi^+ &= \tfrac{1}{12}(+q_{i+3} - 6q_{i+2} + 18q_{i+1} - 10q_i - 3q_{i-1}) \\ q_\xi^- &= \tfrac{1}{12}(+3q_{i+1} + 10q_i - 18q_{i-1} + 6q_{i-2} - q_{i-3}) \end{aligned} \tag{6}$$

And, for fifth-order of accuracy,

$$\begin{aligned} q_\xi^+ &= \tfrac{1}{60}(+2q_{i+3} - 15q_{i+2} + 60q_{i+1} - 20q_i - 30q_{i-1} + 3q_{i-2}) \\ q_\xi^- &= \tfrac{1}{60}(-3q_{i+2} + 30q_{i+1} + 20q_i - 60q_{i-1} + 15q_{i-2} - 2q_{i-3}) \end{aligned} \tag{7}$$

All flows were computed at subsonic freestream speeds. For subsonic inflow/outflow boundaries, the flow variables are evaluated using one-dimensional Riemann-invariant extrapolation. Averaging of the flow variables at the wake cut is performed. At the interface of the viscous and inviscid zone, there is overlapping, and the flow variables at the boundary of each zone are taken from the interior of the adjacent zone.

Results and Discussion

Solutions were obtained for the flow over a double-delta (strake-delta) wing configuration at $M_\infty = 0.22$, $\alpha = 19.0$ deg, and Reynolds number based on the wing chord $Re_C = 4 \times 10^6$. Measurements for the same flow conditions are given in Ref. 10. For all cases, the solution for the near-wall region was obtained with the thin-layer, conservative form of the viscous, compressible flow equations using an implicit scheme and Roe's flux difference splitting. The outer flow was computed as inviscid. For comparison purposes, an inviscid outer solution was obtained with Roe's flux difference splitting and third-order-accurate flux evaluation. Next, the outer inviscid zone was solved with the SCM method using different order of accuracy for the evaluation of the nonlinear inviscid terms as shown in Eqs. (5–7).

An $86 \times 88 \times 64$ point grid along the streamwise, spanwise, and normal directions, respectively, was used as baseline grid. This grid was partitioned into two zones. The inner zone, where the viscous solution was obtained with the conservative scheme, consisted of an $86 \times 88 \times 25$ point grid which included the near-wall viscous

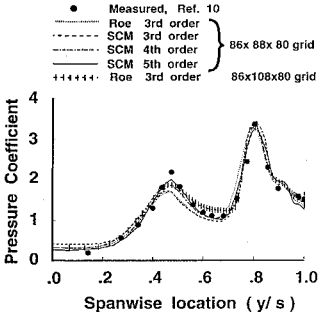

Fig. 1 Effect of the order of accuracy and grid refinement on the prediction of the leeward side surface pressure coefficient distribution at $x/c = 0.65$, $M = 0.22$, $\alpha = 19.0$ deg, $Re_C = 4 \times 10^6$, measurements Ref. 10; third-order conservative solution compared to the third-, fourth-, and fifth-order nonconservative solutions.

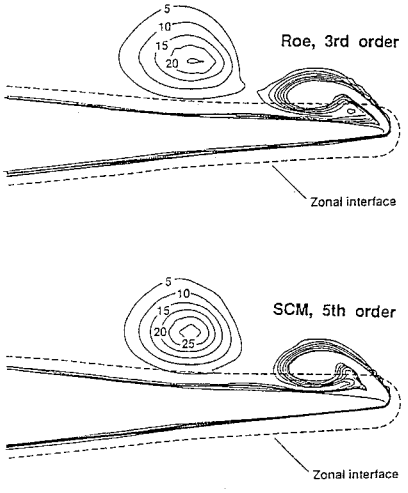

Fig. 2 Effect of the order of accuracy on the prediction of the computed vorticity magnitude at $x/c = 0.65$, $M = 0.22$, $\alpha = 19.0$ deg, $Re_C = 4 \times 10^6$: a) third-order conservative solution and b) fifth-order nonconservative solution.

region and the wake region. The outer inviscid zone consisted of an $86 \times 88 \times 41$ point grid, and extended five wing chord lengths away from the body to the far field. Grid refinement studies were performed with an $82 \times 108 \times 80$ point grid. The refined grid was partitioned in the same way as the baseline grid.

In Fig. 1 the surface pressure coefficient distributions at $x/c = 0.65$, obtained from solutions computed with different orders of accuracy, are compared with the measurements of Ref. 10 and the results obtained from the solution based on the conservative formulation. At the streamwise location $x/c = 0.65$, both the strake and the wing vortices exist. The strake vortex is significantly weaker compared to the wing vortex and has been convected for a distance $l = 0.15c$ from the strake/wing junction. The surface pressure coefficient distributions computed with the conservative and nonconservative formulation and third-order accuracy are in close agreement. The surface pressure distribution obtained from the solution computed using fifth-order accuracy is in closest agreement with the measured values.

To assess the grid resolution required for a lower order solution to reach the accuracy level of a higher order solution, the same flow case was computed on an $86 \times 108 \times 80$ point refined grid. Grid refinement is performed only in the crossflow planes in the region of the strake vortex, where the predictions of the lower order solutions differed the most from the experimentally measured values. Solutions on the refined grid are obtained only with third-order accuracy and the conservative formulation. The surface pressure coefficient distribution obtained from this solution on the refined grid is also compared in Fig. 1 with the surface pressure distributions obtained

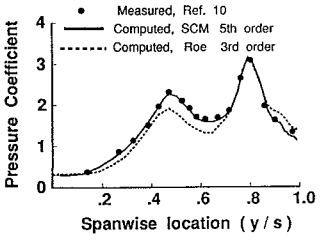

Fig. 3 Effect of the order of accuracy on the prediction of the leeward side surface pressure coefficient distribution at $x/c = 0.65$, $M = 0.22$, $\alpha = 22.4$ deg, $Re_C = 4 \times 10^6$, measurements Ref. 10; third-order conservative solution compared to the fifth-order nonconservative solution.

from the baseline grid using the third-, fourth-, and fifth-order accurate schemes. It is observed that despite the grid refinement, the solution computed on a coarser grid, but with a higher order of accuracy, is in better agreement with the experiment. The vorticity magnitudes in the same crossflow plane at $x/c = 0.65$, obtained with the third-order conservative solution and the fifth-order SCM method solution on the baseline grid are compared in Fig. 2. The vorticity content of the strake vortex predicted by the fifth-order solution is higher.

Next, solutions over the same double-delta wing configuration at a higher angle of incidence, $\alpha = 22.4$ deg, are presented. Solutions were computed on the baseline grid. For this case the strake/wing vortex interaction is stronger and the strake vortex is farther away from the wing surface in the coarser grid region. In addition, vortex breakdown and merging of the strake and wing vortices is observed for a significant portion of the wing section. For the axial location $x/c = 0.65$, however, the strake and wing vortices have not been merged. In Fig. 3 the surface pressure coefficient distribution at $x/c = 0.65$, obtained from the solution computed with fifth order of accuracy, is compared with the measurements of Ref. 10 and the results obtained from the solution based on the conservative formulation and the refined grid. Similar trends with the $\alpha = 19.0$-deg solution are observed for the surface pressure coefficient distributions computed with the conservative and nonconservative formulation and third order accuracy. For this case, however, the discrepancy from the measured values is larger than the $\alpha = 19.0$-deg case. The improvement obtained from the higher order scheme are more noticeable for this case, and it appears that the higher order solution yields uniformly good agreement.

Conclusions

A high-order accurate method on general curvilinear meshes is used to improve the numerical solutions of complex, three-dimensional, vortical flowfields over a sharp-edged double-delta wing at high incidence. The flowfield away from the surface and in the region where the vortex cores are located were computed as inviscid. Higher order of accuracy was obtained using the nonconservative formulation of the compressible equations. The inviscid fluxes were evaluated using third-, fourth-, and fifth-order upwind-biased formulas. The computed results show that a higher order of accuracy enables better convection of vorticity, yields stronger vortices, and produces closer agreement with the measured surface pressures. Grid refinement yields an accuracy level comparable to that obtained from a sparser grid and higher order schemes.

References

[1]Thomas, J. L., Krist, S. T., and Anderson, W. K., "Navier-Stokes Computations of Vortical Flows over Low Aspect Ratio Wings," *AIAA Journal*, Vol. 28, No. 2, 1990, pp. 205–212.

[2]Fujii, K., and Schiff, L. B.,"Numerical Simulation of Vortical Flows over Strake-Delta Wing," *AIAA Journal*, Vol. 27, No. 9, 1989, pp. 1153–1162.

[3]Ekaterinaris, J. A., and Schiff, L. B., "Vortical Flows over Delta Wings and Numerical Prediction of Vortex Breakdown," AIAA Paper 90-0102, 1990.

[4]Ekaterinaris, J. A., and Schiff, L. B., "Navier Stokes Solutions for an Oscillating Double-Delta Wing," AIAA Paper 91-1624, 1991.

[5]Krist, S. L., Thomas, J. L., Sellers, W. L., and Kjelgaard, S. O., "An Embedded Grid Formulation Applied to a Delta Wing," AIAA Paper 90-0429, 1990.

[6]Ekaterinaris, J. A., and Schiff, L. B., "Numerical Investigation of the Effects of Variation of Angle of Attack and Sweep Angle on Vortex Breakdown over Delta Wings," AIAA Paper 91-3000, 1991.
[7]Baldwin, B. S., and Lomax, H., "Thin Layer Approximation and Algebraic Model for Separated Turbulent Flows," AIAA Paper 78-257, 1978.
[8]Courant, R., Isaacson, E., and Rees, M., "On the Solution of Nonlinear Hyperbolic Differential Equations by Finite Differences," *Communications on Pure Applied Mathematics*, Vol. 5, No. 2, 1952, pp. 243–255.
[9]Chakravarthy, S. R., Anderson, D. A., and Salas, M. D., "The Split-Coefficient Matrix Method for Hyperbolic Systems of Gas Dynamic Equations," AIAA Paper 80-0286, 1980.
[10]Cunningham, A. M., and den Boer, R. G.,"Low-Speed Unsteady Aerodynamics of a Pitching Strake Wing at High Incidence—Part II: Harmonic Analysis," *Journal of Aircraft*, Vol. 27, No. 1, 1990, pp. 31–41.

Vorticity in an Inviscid Fluid at Hypersonic Speeds

David Nixon*
The Queen's University of Belfast,
Belfast BT9 5A6, Northern Ireland, United Kingdom

Introduction

OVER the last several years there has been a resurgence of interest in the hypersonic aircraft and in the necessary technologies to make it a feasible proposition. One of the most critical aerodynamic unknowns is the nature of turbulence at very high speeds. There have been investigations into the effects of flow compressibility on turbulence, but most, if not all, of these are directed to extending the knowledge of turbulence at low speeds to incrementally higher speeds. Although this type of approach does yield some useful information, it does not give an indication of the possible magnitude of the problems; namely, what is turbulence in the limit as the Mach number approaches infinity? An attempt to get some indication of turbulence at high Mach numbers is reported by Childs[1] et al. This work was concerned with a numerical simulation of a free shear layer at convective Mach numbers of 4. This study indicated that turbulence at this relatively low Mach number was considerably different from low-speed turbulence. The most notable difference was that the large vortical structures that are a feature of free shear layers inclined at fairly steep angles to the dominant flow direction, in comparison with the situation at low speeds at which the structures are spanwise. However, the free shear layer may not be representative of turbulence in general because of the dominance of the shear layer by large vortical structures, a feature that is not apparent in wall-bounded flows. It is noteworthy that Nixon[2] predicted the appearance of the swept structures using an irrotational model, which may indicate that this feature is not directly connected with turbulence.

There have been other experimental studies of turbulence at high Mach numbers,[3–5] but at very high Mach numbers ($M \sim 10$–20) it is difficult to determine whether it is velocity fluctuations (the dominant factor in low-speed turbulence) or density and pressure fluctuations that are being measured.

This Note describes a simple analysis of vorticity evaluation at high Mach numbers. Since vorticity is the cornerstone of classical turbulence theories, it is helpful to establish whether these theories can be valid at very high Mach numbers. Since analysis of turbulence itself is almost impossible, a simple model problem is posed, namely, the steady flow of an inviscid fluid with constant total enthalpy (h_0) but with an arbitrary prescribed initial vorticity. It is assumed that the fluid can be accelerated isentropically to a very high Mach number where it becomes steady. Although inviscid, the model problem does relate to turbulence, since large-scale turbulence is more or less independent of viscosity.

Received Oct. 15, 1993; accepted for publication March 19, 1994.

*Department of Aeronautical Engineering.

Analysis

It is assumed in the analysis that in the region of interest the flow quantities are small perturbations from reference values, denoted by the subscript r; this will give at least a first-order effect. The density is denoted by ρ, temperature by T, specific enthalpy by h, pressure by p, and entropy by S. The gas constant is denoted by R and the total velocity by q. For a steady flow, with constant total specific enthalpy, the Euler equations can be combined with Gibbs equation to give the following relationships:

$$\frac{\rho}{\rho_r} = \left[1 + \frac{(\gamma-1)}{2} M_r^2 (1 - q^2)\right]^{\frac{1}{(\gamma-1)}} \exp(-S/R) \tag{1}$$

$$\frac{T}{T_r} = \left[1 + \frac{(\gamma-1)}{2} M_r^2 (1 - q^2)\right] \tag{2}$$

$$\frac{p}{p_r} = \left[1 + \frac{(\gamma-1)}{2} M_r^2 (1 - q^2)\right]^{\frac{\gamma}{\gamma-1}} \exp(-S/R) \tag{3}$$

where γ is the ratio of specific heats. The velocity q is normalized with respect to a reference value q_r and has components in a Cartesian coordinate system (x, y, z) of u, v, w.

Let q' be a turbulent velocity fluctuation about q_r and normalized by q_r, that is,

$$q^2 = 1 + 2(u_r u' + v_r v' + w_r w') + u'^2 + v'^2 + w'^2 \tag{4}$$

where u_r, v_r, and w_r are the normalized velocity components of q_r.

Now let

$$\begin{aligned} \rho/\rho_r &= 1 + \rho' \\ T/T_r &= 1 + T' \\ p/p_r &= 1 + p' \\ S/R &= S_0/R + S'/R \end{aligned} \tag{5}$$

where S_0/R is the (constant) reference value of entropy. This implies that the reference flow is irrotational.

If the reasonable assumption that the general fluctuating quantity f' satisfies

$$|f'| \ll 1 \tag{6}$$

is made, then for p/p_r to be real and nonzero,

$$\frac{(\gamma-1)}{2} M_r^2 (q^2 - 1) < 1 \tag{7}$$

or

$$0 \leq 1 + u_r u' + v_r v' + w_r w' + (u'^2 + v'^2 + w'^2)/2 < 1/\left[(\gamma-1)M_r^2\right] \tag{8}$$

If Eq. (6) is applied, Eq. (8) becomes, to first approximation,

$$0 \leq u_r u' + v_r v' + w_r w' < 1/\left[(\gamma-1)M_r^2\right] \tag{9}$$

If the flow is such that $|u_r| \gg |v_r|, |w_r|$, that is, the dominant flow is in the x direction, then Eq. (9) indicates that

$$|u_r u'| \to 0 \text{ as } M_r \to \infty \tag{10}$$

which shows that the fluctuations become two dimensional in the plane normal to the streamwise direction.